

## ARTICLES

**Fluorescence and EPR Characteristics of Mn<sup>2+</sup>-Doped ZnS Nanocrystals Prepared by Aqueous Colloidal Method**

N. Murase,<sup>\*,†</sup> R. Jagannathan,<sup>†,‡,§,||</sup> Y. Kanematsu,<sup>‡,⊥</sup> M. Watanabe,<sup>‡</sup> A. Kurita,<sup>‡,#</sup> K. Hirata,<sup>‡,∇</sup> T. Yazawa,<sup>†,×</sup> and T. Kushida,<sup>‡,∞</sup>

Department of Optical Materials, Osaka National Research Institute, Ministry of International Trade and Industry, Ikeda, Osaka, 563-0026, Japan, Department of Physics, Osaka University, Toyonaka, Osaka, 560-0043, Japan, and Central Electrochemical Research Institute, Karaikudi-630006, India

Received: June 30, 1998; In Final Form: December 10, 1998

Fluorescence properties have been studied for Mn:ZnS crystallites with average diameter of 4 nm prepared by an aqueous colloidal method under 266 nm light excitation. The intensity ratio of the blue band at ~430 nm to the orange band at ~590 nm has decreased after the preparation on a time scale of hours in aqueous solution. On the other hand, hyperfine structures of Mn<sup>2+</sup> in the electron paramagnetic resonance spectrum have increased markedly on the same time scale in solution samples. These phenomena are attributed to the redistribution of defect centers in nanocrystals. Such phenomena have not been observed in samples incorporated into poly(vinyl alcohol). The orange emission is mainly due to the <sup>6</sup>A<sub>1</sub> ← <sup>4</sup>T<sub>1</sub> transition of Mn<sup>2+</sup>, while the blue emission is tentatively assigned to the donor–acceptor pair transition in which the acceptor is related to the Zn<sup>2+</sup> vacancy. Fluorescence decay times of the blue and orange bands have been found to be ~10 ns and ~1 ms, respectively, the latter being the same as in the bulk samples. A weak fluorescent component with fast kinetics observed in the orange region has been identified as a tail of the blue band. No lifetime shortening of the Mn<sup>2+</sup> emission due to quantum confinement has been observed, contrary to reports in the literature.

**I. Introduction**

Recently, ultrafine particle systems have attracted much attention owing to their unique nature especially in optical properties.<sup>1</sup> In these systems, the nonlinear optical susceptibility and absorption cross section can be enhanced considerably.<sup>2,3</sup> The recent advances in the size-selective preparation<sup>4</sup> and single-particle spectroscopy<sup>5,6</sup> will certainly promote a better understanding in this field.

Among the optical phenomena in fine-particle systems, the most fascinating one is the lifetime shortening by as much as 5 orders of magnitude without degradation of fluorescence efficiency. This phenomenon has been observed, for example, in Eu<sup>2+</sup>-doped alkaline earth halides, Eu<sup>2+</sup>-doped chalcogenides,<sup>7,8</sup> and recently in Mn:ZnS.<sup>9</sup> If this effect is actually realized, the optical nonlinear susceptibility as well as optical absorption cross

section is considered to be increased dramatically in transition-doped fine-particle systems. Hence, it will immediately settle various challenging material problems for nonlinear optical applications.<sup>10</sup> However, this effect is still a matter of controversy. It has been reported to be reproducible in Mn:CdS by Qi et al.<sup>11</sup> and in Mn:ZnS by Sooklal et al.<sup>12</sup> In contrast, others report that they did not observe such an effect in Mn:CdS.<sup>13</sup>

In this paper, we aim to clarify the fluorescence decay characteristics and also to study the aging effect in Mn<sup>2+</sup>-doped ZnS nanocrystals prepared by an aqueous colloidal method as reported by Sooklal et al.<sup>12</sup> ZnS is the most typical and important crystalline phosphors both for applications and basic sciences.<sup>14</sup> Following this introductory section, section II explains the experimental details. Electron paramagnetic resonance (EPR) spectroscopy is an excellent probe to gain insight on centers having paramagnetic moments for nanocrystals. On the basis of the results of fluorescence and EPR experiments, we discuss the temporal behavior of defect centers such as Zn<sup>2+</sup> vacancies after the preparation in section III. The origin of the fast-decaying fluorescent component observed in the orange region is also discussed. Finally, section IV concludes this paper.

**II. Experimental Section**

**A. Sample Preparations.** Aqueous samples were prepared in the same way as reported by Sooklal et al.,<sup>12</sup> as briefly described below. Zn(NO<sub>3</sub>)<sub>2</sub>·6H<sub>2</sub>O, Mn(NO<sub>3</sub>)<sub>2</sub>·6H<sub>2</sub>O (Wako pure chemical industries), Na<sub>2</sub>S·9H<sub>2</sub>O, and NaOH (Kishida reagents chemicals) were used without further purification. The water

\* To whom correspondence should be addressed. Telephone: 81-727-51-9642. Fax: 81-727-51-9627. E-mail: n-murase@onri.go.jp.

† Osaka National Research Institute, Japan.

‡ Department of Physics, Osaka University, Japan.

§ Central Electrochemical Research Institute, India.

|| E-mail: cecrik@csecri.res.nic.in.

⊥ Telephone and fax: 81-6-6850-5534. E-mail: kanematu@phys.sci.osaka-u.ac.jp.

# Telephone and fax: 81-6-6850-5534. E-mail: kurita@phys.sci.osaka-u.ac.jp.

∇ Telephone and fax: 81-6-6850-5534. E-mail: khirata@phys.sci.osaka-u.ac.jp.

× Telephone: 81-727-51-9642. Fax: 81-727-51-9627. E-mail: yazawa@onri.go.jp.

∞ Telephone: 81-743-72-6010. Fax: 81-743-72-6019. E-mail: kushida@ms.aist-nara.ac.jp.

employed is normal pure water (JIS A1 grade, prepared by Advantech GS-190) and ultrapure water (JIS A4 grade, prepared by Advantech CPW-100), which were used after degassing by Ar. All the stock solutions were freshly prepared for each experiment. The molar ratio of Mn to Zn was set at an optimum concentration of 2%.

The typical method for preparing Mn:ZnS nanocrystals is as follows. Aqueous solutions (20 mM or 2 mM) of Zn(NO<sub>3</sub>)<sub>2</sub>, Mn(NO<sub>3</sub>)<sub>2</sub>, and Na<sub>2</sub>S were produced first. Zn(NO<sub>3</sub>)<sub>2</sub> (24.5 mL) and Mn(NO<sub>3</sub>)<sub>2</sub> (0.5 mL) were mixed together and set to pH 10.3 by adding aqueous NaOH. The OH<sup>-</sup> ion in the aqueous solution is supposed to adsorb onto the surface of nanocrystals and prevent condensation of each nanocrystal.<sup>12</sup> However, as the pH was increased from the initial value (~6), a slightly white gel was formed, which is attributed to Zn(OH)<sub>2</sub>. After setting the pH to 10.3, Na<sub>2</sub>S (25 mL) was added to the mixed solution at a constant rate (~0.5 or ~8 mL/s) with stirring at a fixed speed in a controlled atmosphere (Ar or air). At this stage, the solution turned turbid because of the formation of Mn:ZnS nanocrystals. The stirring was continued for an additional 10 min to ensure the completion of reaction.

It is not easy to make EPR and fluorescence measurements, especially at cryogenic temperatures, for nanocrystals immediately after the preparation. Therefore, to investigate the aging effect of the nanocrystals, we also prepared samples doped into poly(vinyl alcohol) (PVA). For this purpose, the above-prepared ZnS solution was added to an aqueous solution of PVA (degree of polymerization 1500, Wako pure chemical industries) immediately after the preparation and was cast in a Petri dish.

**B. Observation and Measurements.** The image of the nanocrystal was observed by a transmission electron microscope (TEM, Hitachi, H-9000). X-ray diffraction patterns (Cu K $\alpha$  line) were obtained by an X-ray diffractometer (Rigaku, Geigerflex). Diffraction peaks were assigned by using a standard JCPDS database. Absorption spectra were obtained by a conventional UV-vis spectrophotometer (Hitachi 330). EPR measurements were made at 3 or 77 K with the help of a Bruker ESP 300E X-band (9.60 GHz) ESR spectrometer. The magnetic field corrections were made with a DPPH standard. The signals were averaged over 16–64 scans, depending on the signal quality.

For the fluorescence measurements, samples were excited with the fourth (266 nm) harmonic of a Nd:YAG laser (Spectra-Physics, GCR 130). The time duration, the repetition rate, and the energy of the excitation light pulse were less than 7 ns, 10 Hz, and less than 100  $\mu$ J, respectively. The fluorescence detection was made through a monochromator (Acton Research Corporation, Spectra-Pro 275) with an integrated CCD system in which a time-gated image intensifier (Princeton, Intensifier/18mm/G) was coupled by use of lenses to a liquid-nitrogen-cooled CCD (Princeton LN/CCD-1024-E). The excitation beam was focused on the sample through a lens with a focal length of 10 cm. By changing the lens position, we confirmed that the spectra do not depend on the excitation intensity and the size of the exciting spot. The time resolution of the detection was varied from ~10 ns to 1 ms by applying high-voltage pulses of a given duration to the image intensifier. The position of the time gate relative to the excitation pulse was scanned, and the time-resolved spectrum at each time position was obtained by accumulating enough data to give a good signal-to-noise ratio. A conventional fluorometer (Hitachi F-4500) was also used to measure fluorescence and photoluminescent excitation spectra.

### III. Results and Discussion

**A. X-ray Diffraction and Transmission Electron Microscope Analyses.** The X-ray diffraction pattern of a room-

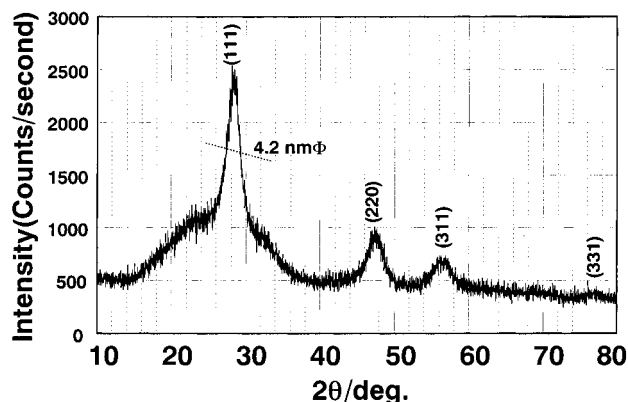


**Figure 1.** X-ray diffraction pattern of the Mn:ZnS (20 mM) nanocrystals prepared by the aqueous colloidal method. Mean particle size is also given.

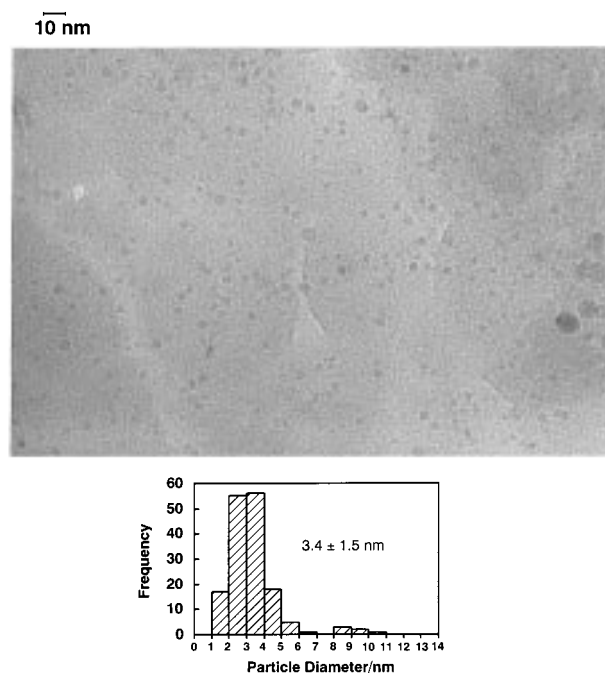


**Figure 2.** Transmission electron microscope image of the same sample as in Figure 1. The histogram in the figure shows the distribution of all of the particles in the picture.

temperature-dried 20 mM ZnS sample is shown in Figure 1. The four peaks observed are assigned to ZnS (sphalerite phase). The mean particle size is estimated to be 4.2 nm by using the Debye–Scherrer formula.<sup>15</sup> The broad peak around 25° is the diffraction from the substrate glass. The particle size of ZnS was almost the same for various samples with different preparation conditions such as the concentration of ZnS, rate of the Na<sub>2</sub>S addition, and the time after the preparation. Figure 2 shows a TEM image of the same sample. The histogram in the figure shows the distribution of all of the particles in the picture. The mean diameter and distribution are calculated to be 3.4 ± 1.5 nm. Therefore, we estimate the particle size to be ~4 nm. This means that the dominant portion of the particles is smaller than the Bohr diameter (~5 nm).

To get direct evidence of the structural relaxation in ZnS particles described in the EPR section later, we have checked the X-ray data measured immediately after the preparation and for a several-day-old sample. However, we could not find any differences in the peak positions and line widths.

**B. UV-Visible Absorption Spectrum.** The bold curve (curve A) in Figure 3 shows the absorption spectrum of a 2

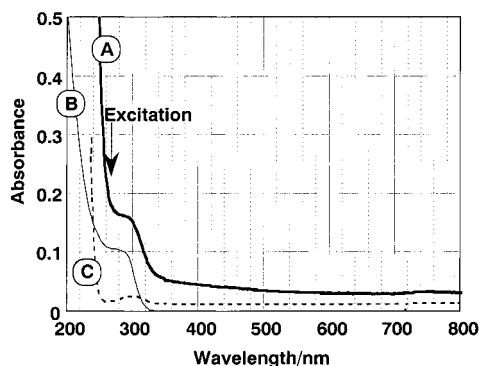


**Figure 3.** Absorption spectrum of 2 mM Mn:ZnS colloidal solution (bold curve A). The contribution of  $\text{HNO}_3$  absorption in the solution is also shown by broken curve C. The excitation wavelength used for the fluorescence measurement (266 nm) is indicated by an arrow. Solid curve B is the absorption spectrum of aqueous solution of ZnS particles (mean diameter of 1.5–3.0 nm) reported by Brus et al., although partially agglomerated.<sup>17</sup> The absolute value of the absorbance was changed by a factor of about 0.15 to adjust the scale of the present data.

mM ZnS sample. The obvious peak at  $\sim 290$  nm is from the ZnS nanocrystals,<sup>16</sup> which is blue-shifted from  $\sim 320$  nm for the bulk because of quantum confinement. For comparison, we show by curve B an absorption of an aqueous solution of ZnS particles (mean diameter of 1.5–3.0 nm) reported by Brus et al., although the particles are partially agglomerated.<sup>17</sup> Both the absorption edge and peak position are quite similar between curves A and B. This also supports that the mean diameter of the present ZnS particle is  $\sim 4$  nm. Sooklal et al.<sup>12</sup> reported a time-dependent red shift of the absorption band of ZnS nanocrystals and attributed it to the particle size growth after the preparation. However, the shift was not observed in our case. Further, we confirmed through TEM and X-ray diffraction analyses that there is no appreciable particle size change due to aging.

After the preparation, the nanocrystals are considered to start precipitation together with the  $\text{Zn}(\text{OH})_2$  gel. This results in the reduction of absorbance of ZnS nanocrystals at 290 nm. Accompanied by this reduction, Sooklal et al. observed that the absorption peak shifts to 300 nm, which was attributed to the particle size growth. However, we interpret this result in a different way. The broken curve C in Figure 3 shows the absorption spectrum of  $\text{HNO}_3$  at the same concentration ( $\sim 1$  mM in the solution). The  $\text{NO}_3^-$  absorbs at 300 nm, which is assigned to an  $n \rightarrow \pi^*$  transition.<sup>18</sup> Owing to the precipitation of the nanocrystals, the relative absorbance at 300 nm becomes stronger with time. We consider that this is the origin of the reported red shift in the literature. Sooklal et al.<sup>12</sup> also stated that they did not observe, at least clearly, the particle size growth by TEM.

**C. Electron Paramagnetic Resonance Spectra.** Figure 4 shows the EPR spectra of the 20 mM aqueous sample at 77 K as a function of time after the preparation. Within 2 h after the preparation (Figure 4a), only the fine structure transition with a  $g$  value of  $\sim 2$  corresponding to the free electron value is observed. After 1 day, the hyperfine structure (hfs) gradually appears as shown in Figure 4b. Two days later, the typical  $\text{Mn}^{2+}$  hfs is clearly observed as in Figure 4c. Accompanied by this aging, the width of the fine structure line becomes narrower, as seen in these figures. This hfs did not change even after 2 months.

Figure 5 shows the EPR spectrum of the 20 mM aqueous sample (2 days old) at 3 K and its enlarged version. The well-

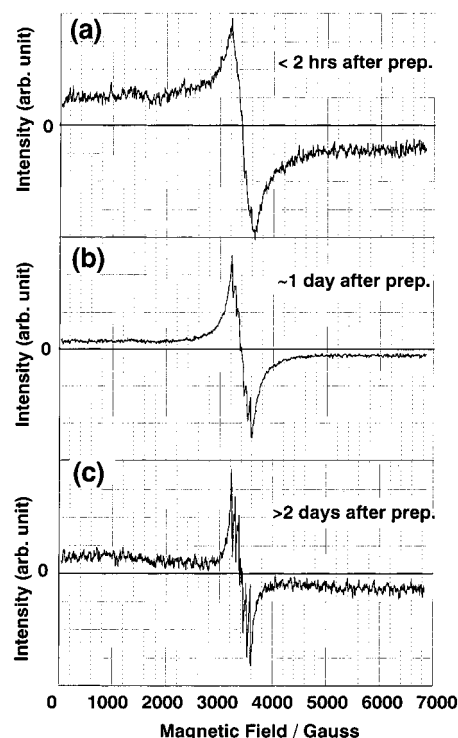


**Figure 4.** EPR spectra at 77 K of the 20 mM aqueous Mn:ZnS sample at (a) 2 h, (b) 1 day, and (c) 2 days after the preparation.

resolved 6-fold structure is consistent with  $\text{Mn}^{2+}$  (nuclear spin  $I = 5/2$  with 100% abundance), and it matches well with that reported recently for a differently prepared methacrylic acid added Mn:ZnS system.<sup>19</sup> From Figure 5b, the EPR parameters for the  $\text{Mn}^{2+}$  center are obtained as  $g = 2.01$  and hyperfine constant  $A = 69.6$  G. These values compare well with those known for the corresponding bulk system.<sup>20</sup> The additional substructure in Figure 5b, which is quite reproducible, can be attributed to the presence of  $\text{Mn}^{2+}$  centers of two different configurations. The possibility of this substructure being the effect of superhyperfine interactions due to the  $\text{S}^{2-}$  ligands surrounding the  $\text{Mn}^{2+}$  center can be discounted because the isotopic abundance of the  $\text{S}^{2-}$  nuclei with nonzero nuclear spin is too small ( $< 1\%$ ) to account for such an intense substructure.

There are two weak signals at a higher  $g$ -value (lower magnetic field) region, as indicated by stars in parts a and c of Figure 5. These signals were not observable at higher temperatures above 77 K. These weak signals at the higher  $g$ -value region are assigned to hole centers.<sup>14</sup> The samples incorporated into PVA exhibited stronger signals at the higher  $g$ -value region, while they showed no hfs at the  $g \approx 2$  region. These features did not change even on a time scale of months after the preparation.

Stoichiometric  $\text{Zn}^{2+}$  and  $\text{S}^{2-}$  were added to the preparation at higher pH. Therefore,  $\text{Zn}^{2+}$  vacancies are considered to be created in the nanocrystals through the formation of a  $\text{Zn}(\text{OH})_2$  gel. Such vacancies should be compensated by the predominantly present  $\text{Na}^+$  in the solution or by the formation of  $\text{S}^-$  ( $\text{S}^{2-} + \text{hole}$ ). Since the thus-produced centers are of acceptor type, they will make hole traps near the valence band edge of ZnS. It is probable that this type of hole center is responsible for the weak signals in the higher  $g$ -value region of parts a and c of Figure 5.

The observed remarkable time dependence of the hfs of the  $\text{Mn}^{2+}$  center can be explained by two possibilities: (i) gradual progress of core polarization<sup>20</sup> of  $\text{Mn}^{2+}$  ( ${}^6\text{S}_{5/2}$  ground state) by

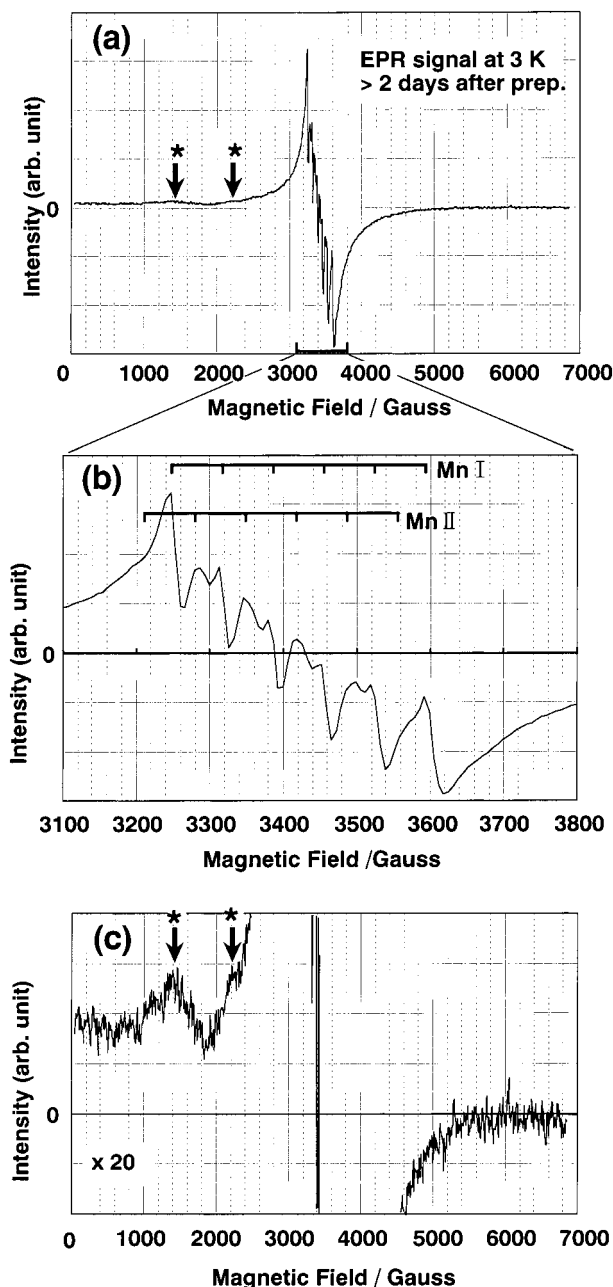


**Figure 5.** (a) EPR spectrum of the same sample as in Figure 3C at 3 K. Stars in the figure at the higher  $g$ -value region show the signals from hole-related centers. (b) An enlarged version of the square bracket region of part a. The bars denote the typical hfs of Mn<sup>2+</sup>. (c) The same figure as in part a but with the vertical axis enlarged 20 times to illustrate the presence of hole centers.

the agglomeration during aging, with the core polarization breaking down the spherical symmetry of the charge distribution; (ii) gradual decrease of the number of various types of defect centers, with the defect centers smearing the hfs on account of additional random perturbation.

The spin distribution of the half-filled Mn<sup>2+</sup> will not have a perfect spherical symmetry even if the particle is about a nanometer or less at the first stage of the preparation. Further, we did not observe appreciable particle size growth due to aging as mentioned before. On the other hand, there are hole-related centers in the course of aging as observed in the higher  $g$ -value region of the EPR spectrum. These centers are considered to be distributed randomly in the nanocrystals immediately after the preparation and perturb the energies of the hyperfine components of Mn<sup>2+</sup>. As a result, the hfs will be smeared out

by the inhomogeneous broadening effect. As time goes, these defect centers will decrease and be distributed uniformly probably through a surface-related structural relaxation. Thus, the hfs appears with time. This is consistent with the observation of a considerable decrease in the line width of hfs due to aging. Hence, we adopt possibility ii in our case. The core polarization brings about a fine splitting even at zero magnetic field. This zero-field splitting and its time dependence may give further information about the symmetry around Mn.

It is reasonable that this structural change accompanies a surface relaxation because the fraction of atoms on the surface position of a particle of this size is estimated to be  $\sim 50\%$ . In the PVA-fixed sample, however, this change will not occur on account of the interaction between the surface of the crystal and the matrix. This explains the fact that the higher  $g$ -value signals do not lose intensity for a long time after the preparation in the samples incorporated into PVA. It is probable that PVA fixes the surface condition of the nanocrystals by hydrogen bonding and does not allow further relaxation.

The fine structure line widths become narrower from part a to part c of Figure 4 with the aging. This is also considered to be a result of rearrangement of defect centers, and accordingly, it supports the appropriateness of interpretation ii. The absence of hfs in Mn<sup>2+</sup> was also reported previously in X-ray irradiated LiH by Ikeya et al.,<sup>21</sup> although they did not definitely clarify the origin of this phenomenon.

Senna et al.<sup>19</sup> showed the importance of methacrylic acid in observing the well-resolved hfs in Mn:ZnS. They concluded that methacrylic acid plays a role in dispersing the Mn<sup>2+</sup> ions and prevents them from forming a dimer. However, we consider that the surface of the nanocrystal is passivated by the addition of methacrylic acid.<sup>9</sup> This also reduces the defect centers around Mn<sup>2+</sup> and causes the well-resolved hfs through the reduction of perturbation of energies of the hfs levels.

Finally, there is an EPR report of Mn:ZnS prepared by an organometallic method.<sup>22</sup> This system is reported to show the lifetime-shortening effect without degradation of the efficiency. The hyperfine splitting of this system is quite broadened. The authors state that there are two kinds of Mn in the Mn:ZnS nanocrystals (mean diameter of 3.5 nm). One is located inside the crystal or very close to another Mn. The other kind of Mn is located at or near the surface. The latter Mn shows the unusual fluorescence of interest. However, this Mn condition is reported to change over several months because of the degradation of the passivating layer consisting of methacrylic acid.

We have also observed two kinds of Mn on the same scale as that of the nanocrystals, although the hyperfine splitting pattern is quite sharp and there is no lifetime-shortening effect as mentioned in the next section. The unusual fluorescence of interest might be observed in some specific cases, such as from a nanocrystal of lower symmetry than cubic and from a dopant located at or near the surface of the nanocrystal, which is well covered by some kinds of surfactant. Though Bhargava et al.<sup>9</sup> ascribed the lifetime shortening to efficient energy transfer from the sp state to the d state taking place in the excited state by enhanced coupling between these states, the clear 6-fold structure (for the both sites) is against such a coupling in the ground state. Whether the several-months-old sample, which does not show an obvious hyperfine signal from the surface Mn, exhibits the same lifetime-shortening effect or not is an important piece of information for elucidating the fluorescence mechanism. Further, we point out that there should be at least an appreciable amount of fluorescence component showing the bulklike Mn<sup>2+</sup> emission because EPR data clearly indicate the

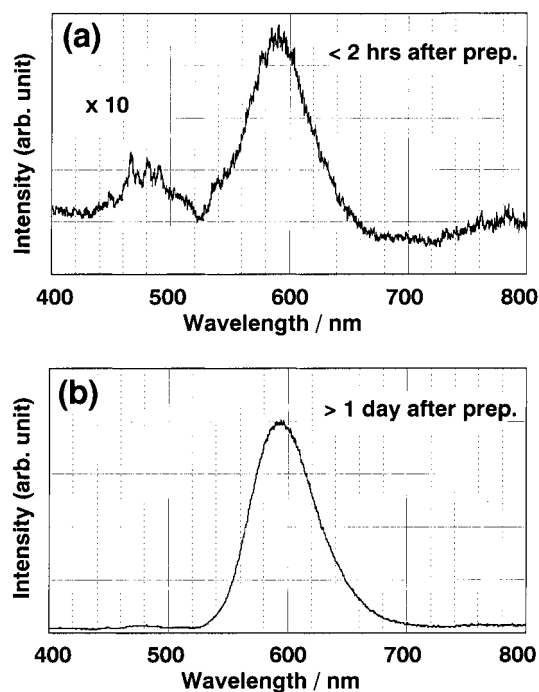


**Figure 6.** Example of fluorescence spectrum of Mn:ZnS solution as a function of time. In this case, the solution (concentration of 20 mM) was prepared using ultrapure water (JIS A4 grade) in Ar atmosphere with slow addition of  $\text{Na}_2\text{S}$  ( $\sim 0.5$  mL/s): (a) 2 h after the preparation; (b) 1 day after the preparation. The vertical axis of part a is expanded 10 times because of the weak fluorescence.

existence of  $\text{Mn}^{2+}$  located at the bulklike position (in cubic sites, not in an axial site), although there are no descriptions in the paper.<sup>9</sup> Finally, our observation that the PVA polymer-fixed Mn:ZnS nanocrystalline sample does not show any hyperfine splitting also demonstrates the importance of the surface conditions of the samples. Senna et al.<sup>19</sup> reports that the methacrylic acid is indispensable for the hyperfine splitting of Mn, but Bhargava's sample did not show this splitting with methacrylic acid in the same X-band measurement.<sup>22</sup>

**D. Fluorescence Properties.** Parts a and b of Figure 6 show the fluorescence spectra of a Mn:ZnS solution sample (20 mM) at 2 and 24 h after the preparation. The spectra consist of two bands at 470 and 590 nm. The 470 nm band sometimes shifts between 430 and 470 nm, although the origin is not clear. This blue emission is observed even in undoped ZnS nanocrystals. The orange emission is mainly due to the  ${}^6\text{A}_1 \leftarrow {}^4\text{T}_1$  transition of  $\text{Mn}^{2+}$ , while the blue band is considered to be related to defect centers.

To clarify that the orange emission is from  $\text{Mn}^{2+}$  in nanocrystals, we measured photoluminescent excitation spectra. A typical case for the detection at 590 nm is shown in Figure 7 together with the spectrum of a commercial bulk-powder Mn:ZnS from Kasei Optonix, Ltd. (type KX-605A, Mn content of 0.45 wt %). The peak position for the nanocrystal is considerably shifted toward the blue because of a confinement effect. The peak wavelength (310 nm) matches well with the absorption spectrum peak shown in Figure 3. Further, this value is quite similar to the previously reported one (309 nm) by Bhargava et al.<sup>23</sup> This clearly indicates that the orange emission is from  $\text{Mn}^{2+}$  situated in nanocrystals. There is a component even around 270 nm in Figure 7. This may be interpreted in terms that even very small ZnS nanocrystals contain  $\text{Mn}^{2+}$  and emit.

So far, there have been many reports about the origin of the blue emission band of ZnS upon ultraviolet irradiation. Kasai et al.<sup>24</sup> measured EPR of a self-activated bulk sample and

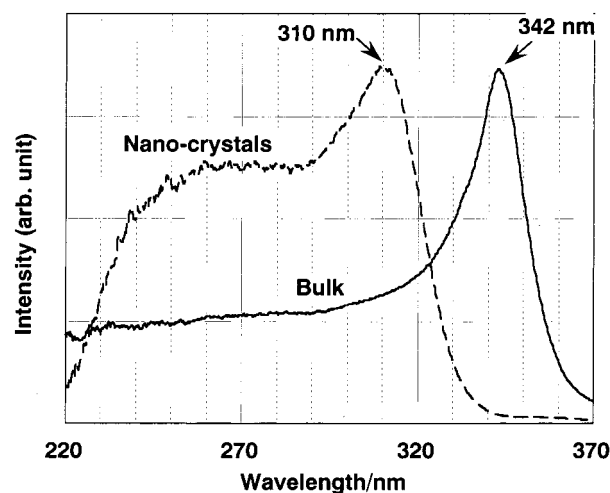


**Figure 7.** Typical photoluminescent excitation spectra of Mn:ZnS nanocrystals (2 mM solution, 2 h after the preparation) and commercial bulk-powder Mn:ZnS. The detection wavelength is 590 nm. A UV cutoff filter was set to the detection side to cut off wavelengths shorter than 340 nm.

reported the existence of fluorescence centers of  $\text{Zn}^{2+}$  vacancy at  $g > 2$  region and those of  $\text{S}^{2-}$  vacancy at  $g < 2$  region, both emitting in the blue. Uchida<sup>25</sup> studied fluorescence properties of bulk samples in correlation with the off-stoichiometry of Zn and S. He concluded that both excess  $\text{Zn}^{2+}$  and  $\text{S}^{2-}$  samples emit at  $\sim 350$  nm by UV irradiation. However, fluorescence at 395 nm was observed only in  $\text{Zn}^{2+}$  excess samples. Becker et al.<sup>26</sup> studied fluorescence from ZnS ( $\sim 100$  nm in diameter) prepared by a colloidal method different from ours. They concluded that the origin of fluorescence at 428 nm is the  $\text{S}^{2-}$  vacancy mainly because of the following three reasons. (1) Uchida assigned<sup>25</sup> the fluorescence at 395 nm to be an  $\text{S}^{2-}$  vacancy origin. (2) The sample made by Becker et al. must have many  $\text{S}^{2-}$  vacancies. This is because the existence of  $\text{S}^{2-}$  in the solution is indicated by the increase of pH in the case of a stoichiometric addition of  $\text{Na}_2\text{S}$  into a  $\text{Zn}^{2+}/\text{Mn}^{2+}$  solution.  $\text{Na}_2\text{S}$  solutions are strongly alkaline. (3) Becker et al. inverted the way of addition and prepared another sample by pouring a  $\text{Zn}^{2+}/\text{Mn}^{2+}$  solution into a  $\text{Na}_2\text{S}$  solution. This suspension should produce many  $\text{Zn}^{2+}$  vacancies in ZnS particles, and no fluorescence was observed in this case.

We admit the last two reasons. However, we consider it unjustifiable to relate their results to Uchida's report. Because Uchida prepared their  $\text{S}^{2-}$  vacancy bulk sample at a high temperature (950 °C) and pressure (several atmospheres), it is not clear if the crystal phase is the same as that of Becker's particles prepared in a solution. Further, the bulk sample made by Uchida emits at 395 nm, whereas Becker et al. discuss the emission at 428 nm. It is reasonable that the emission shifts to the blue in nanocrystals by quantum confinement.

In our case, on the other hand, the synthesis was carried out at higher pH ( $\sim 10$ ) compared to the case of Becker (pH  $\sim 7$ ). This higher value of pH will certainly lead to the formation of the  $\text{Zn}(\text{OH})_2$  gel, leading to  $\text{Zn}^{2+}$  vacancies in ZnS crystals. The EPR spectra indicate the existence of hole centers such as  $\text{Zn}^{2+}$  vacancies. Further, from the detailed experiments including the polarization measurement on single crystals,<sup>27</sup> the self-activated emission (470 nm) of a bulk sample has been assigned to a donor-acceptor type transition between a shallow donor and a  $\text{Zn}^{2+}$  vacancy-related acceptor.<sup>28,29</sup> The observed red shift of this band with time has also been explained by this mechanism.<sup>30</sup> As will be explained later, the blue emission from

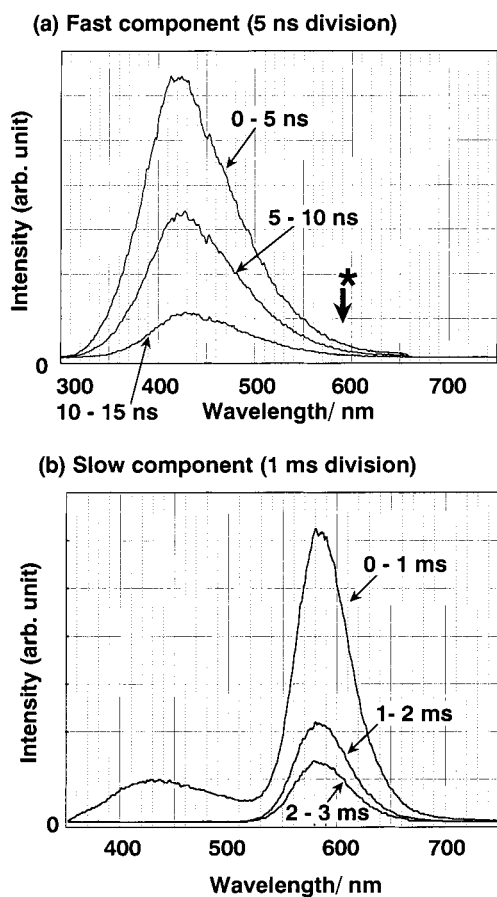


**Figure 8.** (a) Time evolution (5 ns step, first 15 ns after the excitation) of the fluorescence of Mn:ZnS doped into PVA (2.0 mM) upon excitation at 266 nm. The star \* indicates the presence of an orange emission component having a short decay time ( $\sim 10$  ns). (b) Time evolution (1 ms step, first 3 ms after the excitation) of the fluorescence in the same sample.

our nanocrystals shows the same red shift with time as in Figure 9b. Therefore, we tentatively assign the blue band at 430–470 nm to the donor–acceptor pair transition in which the acceptor is related to the Zn<sup>2+</sup> vacancy. The energy position of this band is blue-shifted compared to the self-activated emission in the bulk ZnS. This is consistent with the quantum confinement effect in nanocrystals.

We notice that the intensity ratio of the blue emission to the orange changes considerably with time after the preparation. This observation coincides with that reported by Sooklal et al.<sup>12</sup> As for the absolute fluorescence intensity, the orange emission increases by about 1 order of magnitude within 1 day, while the blue band is rather insensitive to time. Sometimes, the blue emission intensity decreased with time in accordance with the report of Sooklal et al.<sup>12</sup> However, the precise comparison is difficult because the absolute fluorescence intensity depends on the amount of the solution and the Zn(OH)<sub>2</sub> gel in the cell. This is considered to be due to the fact that the gel in the solution precipitates during the measurement together with the nanoparticles.

The time-dependent increase in the orange emission can be explained as follows. As explained in section III.C, there are randomly distributed defect centers in the nanocrystals at the early stage of preparation. Hence, the fluorescence efficiency of Mn<sup>2+</sup> inside the crystal is low because the excitation energies are transferred into the defect centers in the vicinity of Mn<sup>2+</sup> ions. These defect centers will move to the surface, and its number in the crystal will decrease with time in the colloidal

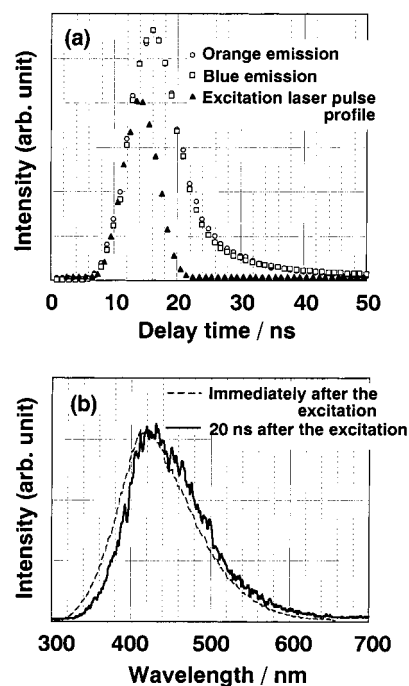


**Figure 9.** (a) Intensity-normalized fluorescent decay curves in both the blue and orange regions together with the excitation laser pulse profile. (b) Intensity-normalized fluorescence spectrum immediately after the excitation and that at 20 ns after the excitation.

solution. This structural relaxation explains the temporal increase in the fluorescence efficiency of Mn<sup>2+</sup>.

When the sample was incorporated into PVA, the fluorescence efficiency did not change appreciably with time even when heat-treated at 60 °C for 2 days. This time invariance coincides with the EPR results of these samples and can be explained by the absence of the time-dependent structural change in nanocrystals fixed in PVA. Thus, this result supports the above explanation.

One of the main objectives of the present investigation is to clarify whether the lifetime-shortening effect of Mn<sup>2+</sup> emission exists or not in Mn:ZnS nanocrystals. We studied the time behavior of fluorescence for various samples including those fixed in PVA. Parts a and b of Figure 8 show the time evolution of the fluorescence spectra after the excitation of 2.0 mM Mn:ZnS in PVA as an example. Figure 8a is on the time scale of 5 ns, whereas Figure 8b is on the time scale of 1 ms. From these results, the fluorescence decay time of the blue emission was obtained as  $\sim 10$  ns while that of the orange emission as  $\sim 1$  ms, which is the same as in the bulk samples.

Since there exists a weak fluorescent component having a short decay time in the orange region as denoted by a star in Figure 8a, we further inspected the time profile of the fluorescence carefully. Figure 9a shows the intensity-normalized fluorescent decay curves at both the blue and orange regions together with the excitation laser pulse profile. We notice that the time profile of the fast orange emission component coincides with that of the blue emission within experimental error. Figure 9b shows the intensity-normalized fluorescence spectrum immediately after the excitation and that at 20 ns after it. The two spectra almost agree with each other, although the latter shifts a little to the red as explained previously. These results clearly prove that the weak fluorescent component with fast kinetics observed in the orange region is a tail of the blue band.

We studied the time behavior of Mn<sup>2+</sup> emission for samples with various preparation conditions, such as the concentration

of ZnS (2 and 20 mM), the purity of the water (JIS A1 and A4 grades), the rate of the addition of Na<sub>2</sub>S (~0.5 or ~8 mL/s), the preparation atmosphere (Ar and air), the time after the preparation (30 min to 1 month), and host matrices (water and PVA). We further compared the results at the top and the bottom portions of the solution. Furthermore, we also measured the fluorescence lifetime at cryogenic temperatures. The blue emission component becomes stronger, but its lifetime increases only about 50%, which is still on the order of nanoseconds. There are some reports<sup>28,29</sup> on self-activated emission from ZnS bulk at low temperatures. All of these values are in microsecond regions. This also supports that our observation is the emission from nanocrystals. In all these cases, no lifetime-shortening effect in Mn<sup>2+</sup> emission reported in the literature was observed. Therefore, we conclude that there is no change in the oscillator strength of Mn<sup>2+</sup> transition due to the quantum confinement in this system. In an earlier experiment,<sup>12</sup> the reported time profiles of fluorescence at fixed wavelengths were only on short time scales (several microseconds at most). The description in the literature shows that attention was paid only on the detection of short-lifetime components, and there is no explanation about the measurement of the millisecond component. We consider that the long-lifetime component did exist but was not measured in the samples in the literature. The most convincing way to find out whether a fluorescent component is due to a tail of another band or not is to measure the spectral profile for each time scale as shown in Figure 8. We also notice that Bhargava et al.<sup>9</sup> did not report such profiles in the first paper on lifetime shortening.

#### IV. Conclusions

Mn:ZnS nanocrystals prepared by the aqueous colloidal method did not show any lifetime-shortening effect in the Mn<sup>2+</sup> emission around 590 nm contrary to the report on the samples prepared by following the same procedure.<sup>12</sup> The short-lifetime component (~10 ns) in the orange region was found to originate from the tail of the blue emission peaked around 430 nm. The time dependence of the hyperfine structure intensity of Mn<sup>2+</sup> in the EPR spectrum and that of the fluorescence intensity ratio of blue to orange in the solution samples were attributed to the redistribution process of defect centers such as that related to Zn<sup>2+</sup> vacancies after the preparation. Such temporal behavior was not observed for the samples fixed in the PVA matrix. It is important to mention that the blue emission was not observed in Mn:ZnS nanocrystals grown by an organometallic method as in the first report by Bhargava et al.<sup>9</sup> Therefore, it is still uncertain whether the lifetime shortening due to quantum confinement is actually present or not in differently prepared Mn:ZnS nanocrystals.

**Acknowledgment.** The authors are grateful to Drs. N. Kitamura and H. Mizoguchi for their help in the EPR experiment and to Dr. M. Haruta for valuable discussion. One of the authors (R.J.) acknowledges gratefully the Japan Society for the Promotion of Science (JSPS) for the award of a fellowship.

#### References and Notes

- (1) Alivisatos, A. P. *Science* **1996**, *271*, 933.
- (2) Wang, Y. *Acc. Chem. Res.* **1991**, *24*, 133.
- (3) Vossmeier, T.; Katsikas, L.; Giersig, M.; Popovic, I. G.; Diesner, K.; Chemseddine, A.; Eychmüller, A.; Weller, H. *J. Phys. Chem.* **1994**, *98*, 7665.
- (4) Dabbousi, B. O.; Rodriguez-Viejo, J.; Mikulec, F. V.; Heine, J. R.; Mattoussi, H.; Ober, R.; Jensen, K. F.; Bawendi, M. G. *J. Phys. Chem. B* **1997**, *101*, 9463.
- (5) Empedocles, S. A.; Norris, D. J.; Bawendi, M. G. *Phys. Rev. Lett.* **1996**, *77*, 3873.
- (6) Tittel, J.; Göhde, W.; Koberling, F.; Basché, Th.; Kornowski, A.; Weller, H.; Eychmüller, A. *J. Phys. Chem. B* **1997**, *101*, 3013.
- (7) Fork, R. L.; Taylor, D. W.; German, K. R.; Kiel, A.; Buehler, E. *Phys. Rev. Lett.* **1974**, *32*, 781.
- (8) Fork, R. L.; Taylor, D. W. *Phys. Rev. B* **1979**, *19*, 3365.
- (9) Bhargava, R. N.; Gallagher, D.; Hong, X.; Nurmikko, A. *Phys. Rev. Lett.* **1994**, *72*, 416.
- (10) Murase, N.; Kushida, T.; Kurita, A.; Kanematsu, Y.; Watanabe, M.; Hirata, K.; Yazawa, T. Japan Patent, H10-48889, February 12, 1998.
- (11) Qi, J.; Okuno, T.; Masumoto, Y. Abstract in Asia symposium on optical properties, Nara, Japan, Nov 1 and 2, 1996; p 333.
- (12) Sooklal, K.; Cullum, B. S.; Angel, S. M.; Murphy, C. J. *J. Phys. Chem.* **1996**, *100*, 4551.
- (13) Chamorro, M. A.; Voliotis, V.; Grousson, R.; Lavallard, P.; Gacoin, T.; Counio, G.; Boilot, J. P.; Cases, R. *J. Cryst. Growth* **1996**, *159*, 853.
- (14) Marfunin, A. S. (translated by Schiffer, V. V.) *Spectroscopy, Luminescence and Radiation Centers in Minerals*; Springer-Verlag: New York, 1979.
- (15) Cullity, B. D. *Elements of X-ray Diffraction*; Addison-Wesley: Reading, MA, 1956; p 99.
- (16) Weller, H. *Angew. Chem., Int. Ed. Engl.* **1993**, *32*, 41.
- (17) Rossetti, R.; Hull, R.; Gibson, J. M.; Brus, L. E. *J. Chem. Phys.* **1985**, *82*, 552.
- (18) *Mellor's Comprehensive Treatise on Inorganic and Theoretical Chemistry*; Longmans: London, 1967; Vol. III, Supplement II, N (Part II), p 479.
- (19) Yu, I.; Isobe, T.; Senna, M. *J. Phys. Chem. Solids* **1996**, *57*, 373.
- (20) Abragam, A.; Bleaney, B. *Electron Paramagnetic Resonance of Transition Ions*; Clarendon Press: Oxford, 1970.
- (21) Ikeya, M. *Phys. Status Solidi B* **1982**, *111*, 525.
- (22) Kennedy, T. A.; Glaser, E. R.; Klein, P. B.; Bhargava, R. N. *Phys. Rev. B* **1995**, *52*, R14356.
- (23) Gallagher, D.; Heady, W. E.; Racz, J. M.; Bhargava, R. N. *J. Mater. Res.* **1995**, *10*, 870.
- (24) Kasai, P. H.; Otomo, Y. *J. Chem. Phys.* **1962**, *37*, 1263.
- (25) Uchida, I. *J. Phys. Soc. Jpn.* **1964**, *19*, 670.
- (26) Becker, W. G.; Bard, A. J. *J. Phys. Chem.* **1983**, *87*, 4888.
- (27) Koda, T.; Shionoya, S. *Phys. Rev. Lett.* **1963**, *11*, 77. Koda, T.; Shionoya, S. *Phys. Rev.* **1964**, *136*, A541.
- (28) Era, K.; Shionoya, S.; Washizawa, Y. *J. Phys. Chem. Solids* **1968**, *29*, 1827.
- (29) Era, K.; Shionoya, S.; Washizawa, Y.; Ohmatsu, H. *J. Phys. Chem. Solids* **1968**, *29*, 1843.
- (30) Oda, S.; Kukimoto, H. *J. Lumin.* **1979**, *18/19*, 829.